Structural ordering and glass forming of soft spherical particles with harmonic repulsions

Bin Sun, Zhiwei Sun, Wenze Ouyang, and Shenghua Xu

Citation: The Journal of Chemical Physics **140**, 134904 (2014); doi: 10.1063/1.4869833
View online: http://dx.doi.org/10.1063/1.4869833
View Table of Contents: http://scitation.aip.org/content/aip/journal/jcp/140/13?ver=pdfcov
Published by the AIP Publishing

Structural ordering and glass forming of soft spherical particles with harmonic repulsions

Bin Sun,[1] Zhiwei Sun,[2] Wenze Ouyang,[2,a)] and Shenghua Xu[2,b)]
[1]*School of Materials and Chemical Engineering, Zhongyuan University of Technology, Zhengzhou 450007, China*
[2]*Key Laboratory of Microgravity (National Microgravity Laboratory), Institute of Mechanics, Chinese Academy of Sciences, Beijing 100190, China*

(Received 30 December 2013; accepted 11 March 2014; published online 4 April 2014)

We carry out dissipative particle dynamics simulations to investigate the dynamic process of phase transformation in the system with harmonic repulsion particles. Just below the melting point, the system undergoes liquid state, face-centered cubic crystallization, body-centered cubic crystallization, and reentrant melting phase transition upon compression, which is in good agreement with the phase diagram constructed previously via thermodynamic integration. However, when the temperature is decreased sufficiently, the system is trapped into an amorphous and frustrated glass state in the region of intermediate density, where the solid phase and crystal structure should be thermodynamically most stable. © *2014 AIP Publishing LLC*. [http://dx.doi.org/10.1063/1.4869833]

I. INTRODUCTION

Many macromolecules and their self-assembled entities, emulsions, soft colloids, and grains can be regarded as soft spherical particles.[1,2] Over the last decades, more and more studies about the phase behavior of the systems with soft particles have been done using computer simulations, e.g., penetrable spheres model (PSM), Gaussian core model (GCM), Hertzian spheres system, Yoshida-Kamakura (YK) model, and soft spheres with harmonic repulsions.[3–10] Although it has been established by many results that the behavior of soft particles is similar to that of hard ones in vanishing pressure and temperature,[11–13] the phase behavior and crystallization mechanism of soft particles are considered to be qualitatively different from those of hard particles.[14] In general, the diverging repulsions at close separation between the particles are the dominant factors causing crystallization, and the crystal structure into which a system freezes depends on the steepness of the repulsion, with hard repulsions favoring a face-centered cubic (fcc) lattice and soft ones a body-centered cubic (bcc) lattice. For the soft particles, the phase behaviors become more complex because soft particles may elastically deform and even mutually interpenetrate when colliding with each other.

As is well known, the repulsive potentials are necessary to bring about a solidification transition and the shape of the pair potential determines the phase behavior of the system.[14] Nevertheless, the existence of a thermodynamically stable solid phase does not necessarily require a singular repulsion for vanishing interparticle separations. In this respect, it is interesting to consider an extreme class of repulsive potentials that are bounded, i.e., they remain finite for the whole range of interparticle separations, even at full overlap between the particles.[14,15] Many previous works have suggested that the systems with bounded potential have rich phase behaviors. Stillinger and subsequently other authors showed that the so-called GCM has a maximum melting point, and exhibits reentrant melting and a transition from fcc to bcc crystal structures upon compression.[4,5,16] Such a rich phase behavior is not only limited to the GCM, but also has been shown to be common to many other bounded potentials.[8,10] However, not all soft-repulsive potentials give rise to reentrant melting. In the system of the PSM, it was found that no reentrant melting takes place with increasing density because a clustering mechanism stabilizes the solid at all temperatures.[3] Likos *et al.* derived a simple criterion to determine whether a system of bounded potential shows reentrant melting or clustering, by employing a mean-field-density-functional theory: Reentrant melting happens for bounded potentials with a positive definite Fourier transform. Otherwise, clustering and freezing are expected to occur at all temperatures.[17]

As the soft particles with bounded potential have limited short-range repulsions, the repulsive forces may be inversely proportional to distance between the centers of the particles. For this case, a typical model of harmonic spheres is introduced, in which the repulsion between two approaching particles starts when their distance is smaller than the sum of their radii. This model, originally proposed to describe wet foams,[18] has not only become a paradigm in numerical studies of the $T = 0$ jamming transition,[2,19,20] but also been studied at finite temperatures[10,21,22] and finds experimental realizations in emulsions, soft colloids, and grains.[12,23]

In this research, we use a mesoscopic simulation technique, dissipative particle dynamics (DPD), to study the phase behaviors of the system. In a typical DPD simulation, the hydrodynamic behavior is considered, so that the dynamics process of the phase transition in the system can be investigated.[24] There are two kinds of structural ordering in soft particle systems, i.e., fcc and bcc, which were reported and attracted much interest in computational, theoretical, and experimental investigations.[4–8,10,14,25–27] Therefore, fcc and

a)Electronic mail: oywz@imech.ac.cn
b)Electronic mail: xush@imech.ac.cn

bcc phase are mainly considered in the paper, although the constructed phase diagram of the system shows a complex phase behavior and a succession of Bravais crystals especially at very low temperature.[10]

II. MODEL AND SIMULATION METHODOLOGY

The particles interact by the harmonic repulsion, which is given by

$$U(r_{ij}) = \begin{cases} \frac{\epsilon}{2}(1 - r_{ij}/\sigma)^2, & r_{ij} < \sigma \\ 0, & r_{ij} \geq \sigma \end{cases}, \tag{1}$$

where r_{ij} is the distance between ith particle and jth particle. The parameters ϵ and σ govern the strength and maximum distance of the interaction, respectively. For soft spherical particles, the maximum distance of the interaction σ is equal to their diameters.

DPD is a kind of mesoscale simulation technique, which was introduced by Hoogerbrugge and Koelman[28] in 1990s and has been modified over the years.[24,29] We prefer the version of DPD as described in the paper by Groot and Warren[24] due to its greater simplicity. In the following we only give a brief summary of the DPD simulation algorithm since more details can be seen in Ref. 24. The system of beads interacts with each other as a result of pairwise additive forces comprising of conservative forces $\mathbf{F}_{ij}^C$, dissipative forces $\mathbf{F}_{ij}^D$, and random forces $\mathbf{F}_{ij}^R$, written by

$$\mathbf{F}_i = \mathbf{F}_{ij}^C + \mathbf{F}_{ij}^D + \mathbf{F}_{ij}^R \, . \tag{2}$$

In a typical DPD simulation, the conservative force between DPD particles is exactly the same as the interaction of harmonic soft particles, which is given by

$$\mathbf{F}_{ij}^C = \begin{cases} \epsilon(1 - r_{ij}/r_c)\mathbf{e}_{ij} & r_{ij} < r_c \\ 0, & r_{ij} \geq r_c \end{cases}. \tag{3}$$

Here $\mathbf{e}_{ij}$ is the unit vector $\mathbf{e}_{ij} = \mathbf{r}_{ij}/r_{ij}$. Therefore, the DPD can be adopted to equilibrate the systems of isotropic spheres with harmonic repulsions and the cutoff radius of the interaction is chosen as $r_c = \sigma$ in this study.

The dissipative force and random force are defined by

$$\begin{aligned} \mathbf{F}_{ij}^D &= -\gamma\omega^D(r_{ij})(\mathbf{v}_{ij} \cdot \mathbf{e}_{ij})\mathbf{e}_{ij}, \\ \mathbf{F}_{ij}^R &= \eta\omega^R(r_{ij})\zeta_{ij}\delta t^{-1/2}\mathbf{e}_{ij}. \end{aligned} \tag{4}$$

Here ζ_{ij} is a random number with zero mean and unit variance. $\mathbf{v}_{ij} = \mathbf{v}_i - \mathbf{v}_j$. η determines the magnitude of the random force between particles, which is taken to be $\eta = 3.0$ for better temperature control. The relationship between γ and η is $\eta^2 = 2\gamma k_B T$, where k_B is the Boltzmann constant. In order to satisfy fluctuation-dissipation theorem, the weight functions $\omega^D(r_{ij})$ and $\omega^R(r_{ij})$ should follow the relation $\omega^D(r_{ij}) = [\omega^R(r_{ij}]^2$. A simple but useful choice of the weight function $\omega^D(r_{ij})$ is

$$\omega^D(r_{ij}) = \begin{cases} (1 - r_{ij}/r_c)^2, & r_{ij} < r_c \\ 0, & r_{ij} \geq r_c \end{cases}. \tag{5}$$

The modified velocity-Verlet algorithm is used to integrate the equations of motion

$$\begin{aligned} \mathbf{r}_i(t + \delta t) &= \mathbf{r}_i(t) + \delta t\mathbf{v}_i(t) + \frac{1}{2}(\delta t)^2\mathbf{a}_i(t), \\ \mathbf{v}_i'(t + \delta t) &= \mathbf{v}_i(t) + \lambda\delta t\mathbf{a}_i(t), \\ \mathbf{a}_i(t + \delta t) &= \mathbf{a}_i(\mathbf{r}(t + \delta t), \mathbf{v}_i'(t + \delta t)), \\ \mathbf{v}_i(t + \delta t) &= \mathbf{v}_i(t) + \mathbf{v}_i\left(t + \frac{1}{2}\delta t\right)(\mathbf{a}_i(t) + \mathbf{a}_i(t + \delta t)), \end{aligned} \tag{6}$$

where $\mathbf{a}_i = \mathbf{F}_i/m$ is the acceleration of ith particle, and $\lambda = 0.65$ is taken according to the suggestion of Groot and Warren for an accurate temperature control.[24]

DPD simulations are performed in NVT ensemble, where the total number of particles N, the temperature T, and the volume of simulation cell V are kept constant. Period boundary conditions are applied. The reduced units are used in the simulation. The basic units are chosen as follows: energy unit 0.04ϵ, length unit σ, and the mass of particle m. So the parameters ϵ and σ in reduced units are taken the same values as those originally used by Groot and Warren,[24] i.e., $\epsilon^* = 25$ and $\sigma^* = 1.0$, respectively. The temperature in reduced units can be obtained by $T^* = 25k_BT/\epsilon$. Notice here that the superscript $*$ of the parameters in reduced units are omitted for convenience in the following part of the paper. The equation of particles' motion is integrated using velocity-Verlet algorithm as described in Eq. (6) with the time step $\delta t = 0.01$.

During the process of structural ordering or crystallization, we need to distinguish particles that are part of the crystal from those that belong to the liquid. Here we use the method presented by Frenkel and coworkers.[30] In this method, the type of a particle is determined based on its local environment. First we consider the set of nearest neighbors of a particle i as all particles j that are within a given radius r_q from i. The value of r_q is chosen close to the first minimum of radial distribution function (RDF). Then, the complex vector $q_{lm}(i)$ of particle i is defined by

$$q_{lm}(i) = \frac{1}{N_{nb}(i)} \sum_{j=1}^{N_{nb}(i)} Y_{lm}(\mathbf{r}_{ij}) \, . \tag{7}$$

Here $N_{nb}(i)$ is the number of nearest neighbors of particle i. The functions $Y_{lm}(\mathbf{r}_{ij})$ are the spherical harmonics, l is a free integer parameter, and m is an integer that runs from $m = -l$ to $m = l$. To identify solid-like particles, the integer parameter l is taken as $l = 6$ and $q_{6m}(i)$ should be normalized

$$d_{6m}(i) = \frac{q_{6m}(i)}{\left[\sum_{m=-6}^{6} |q_{6m}(i)|^2\right]^{1/2}} \, . \tag{8}$$

Using the normalized complex vectors $d_{6m}(i)$, a scalar product which measures the correlation between neighboring particles i and j can then be defined by

$$S_{ij} = \sum_{m=-6}^{6} d_{6m}(i) \cdot d_{6m}^*(j) \, , \tag{9}$$

where the superscript $*$ indicates complex conjugation. Two neighboring particles i and j are defined to be connected if the scalar product S_{ij} described above exceeds a given value, typically $S_{ij} > 0.7$. In the literatures, different threshold values of S_{ij} have been used for this purpose.[27,30] We do not see any substantial differences in our results when we use 0.5–0.7 as the threshold value of S_{ij}. A particle will be identified as solid-like if the number of connections is above a certain threshold, typically 8. Then, we define the degree of crystallinity $f_{crystal}$ of a sample as the number of particles in solid-like environments divided by the total number of particles N.

Given the definition of Eq. (7), one can construct another bond order parameter

$$w_l = \sum_{m_1+m_2+m_3=0} \begin{pmatrix} l & l & l \\ m_1 & m_2 & m_3 \end{pmatrix} \frac{q_{lm_1}(i)q_{lm_2}(i)q_{lm_3}(i)}{\left(\sum_{m=-l}^{l} |q_{lm}(i)|^2\right)^{3/2}}. \tag{10}$$

Here, the integers m_1, m_2, and m_3 run from $-l$ to l, but only combinations with $m_1 + m_2 + m_3 = 0$ are allowed. The term in parentheses is the Wigner $3j$ symbol. To further identify the solid-like particles, we take advantage of the different symmetries that the crystals have on the w_6 and w_4 axis.[27] So the following criterion for crystal classification is used: first, crystal or solid-like particles are identified using the method presented by Frenkel and coworkers which has been described above. Then, we identify (i) fcc particles as all crystal particles with $w_6 < 0$ and $w_4 < 0$; (ii) hcp particles as all crystal particles with $w_6 < 0$ and $w_4 > 0$; and (iii) bcc particles as all crystal particles with $w_6 > 0$.

III. RESULTS AND DISCUSSION

The system with harmonically repulsive spheres can be crystallized and show a structural ordering below the melting temperature $T_m \approx 0.159$.[10] In the present work, the number of particles is typically chosen as $N = 10\,976(4 \times 14^3)$ to match the number of lattice points for fcc structure in cubic box. The particles are initially placed on random positions and their velocities satisfy the Maxwell-Boltzmann distribution with the temperature $T = 1.0$. After a relaxation of $10^5\delta t$, the system is quenched to the desired temperature and simulations are carried out long enough until the curves of system's properties almost reach a plateau so that a final equilibrium is reached. Most of the typical simulations run over 4×10^6 time steps and the last 10^6 time steps are used for every $100\delta t$ to calculate the average values of some parameters needed. For the simulations close to the phase transition, more time steps, typically $10^7\delta t$, are used to get an equilibrium.

First we set the desired temperature $T = 0.1$. When the density is small, the system exhibits a liquid state as expected. Increasing the density high enough, the particles begin to crystallize and a freezing transition occurs. The evolution of mean square displacement (MSD) with the time steps is displayed in the top panel of Fig. 1. The MSD has an obvious increase since the simulation starts, and then reaches a plateau, which reflects that the system has reached equilibrium and the particles' motion is restricted to their equilibrium positions. In the middle panel of Fig. 1, the evolution of solid-like particles' number during crystallization is given. Starting from the initial random configuration at which most of particles are liquid-like, more and more particles begin to crystallize so that the number of solid-like particles increases apparently. When the system reaches equilibrium, almost all of the particles become solid-like indicating that the system's crystallization is completed. The curve of RDF can be used to analyze the long-range order of the system and distinguish the structure of the resulting crystals. Here we should mention that the pair distance in x axis of RDF curve is divided by the relevant length scale L_0, where $L_0 = \sqrt[3]{\frac{6V}{\pi N}}$, in order for a convenient and clear view of the crystal structure. The bottom panel of Fig. 1 shows the curve of averaged RDF

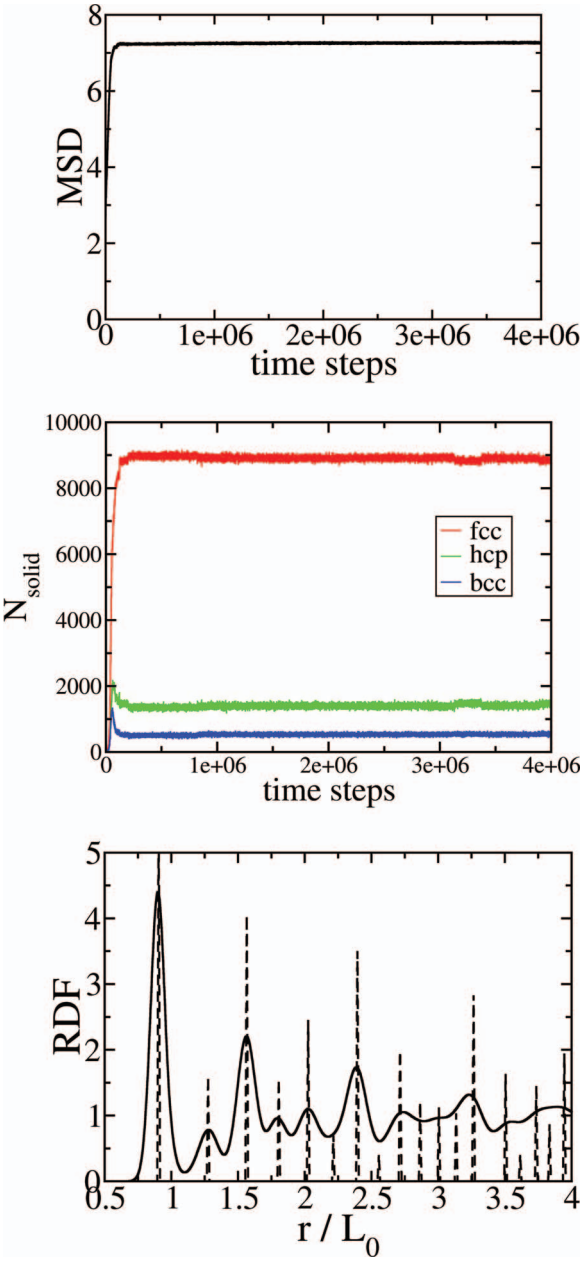

FIG. 1. Crystallization of fcc structure at $T = 0.1$ and $\rho = 1.7$. Top: mean square distance (MSD) versus time step. Middle: the number of different types of solid-like (fcc, hcp, bcc) particles versus time step. Bottom: averaged radial distribution function (RDF) after equilibrium. The dashed lines in RDF curve indicate the peaks of perfect fcc crystal structure.

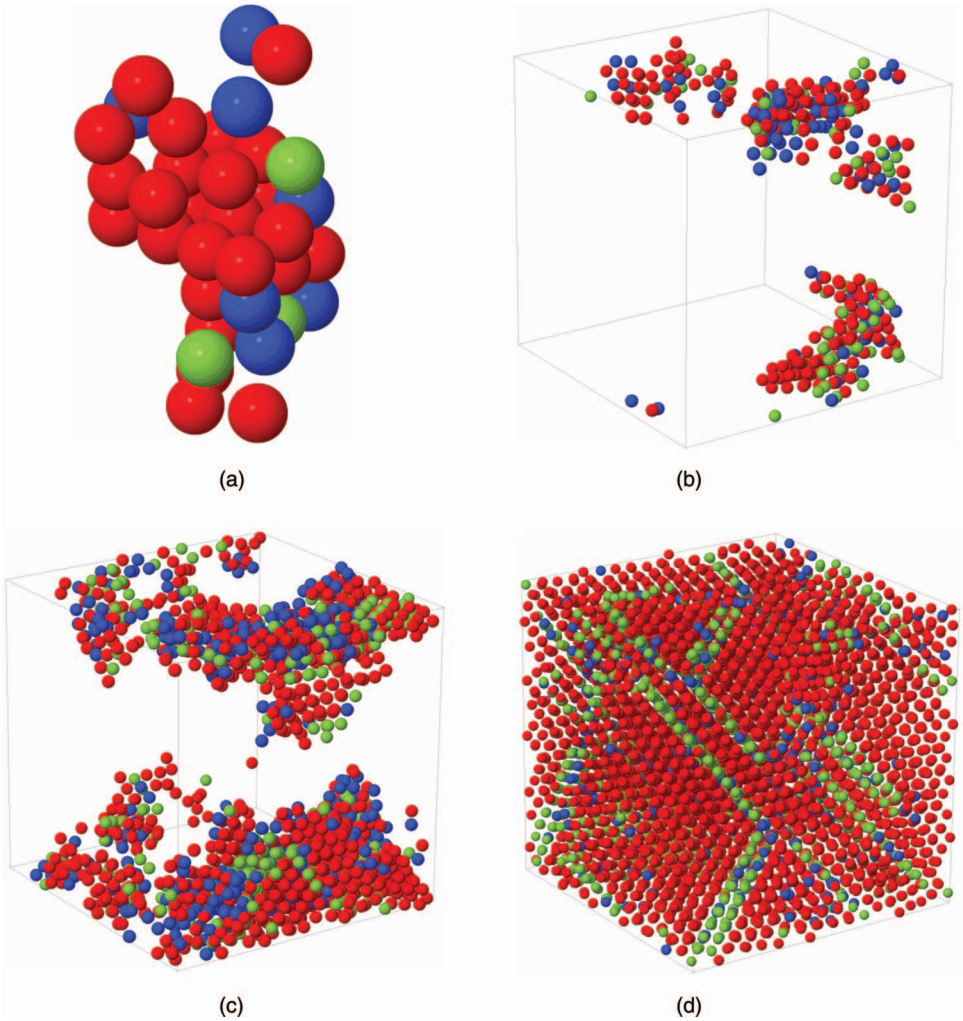

FIG. 2. Snapshots of fcc crystallization at $T = 0.1$ and $\rho = 1.7$. Red, green, and blue spheres represent fcc, hcp, and bcc particles, respectively. (a) The largest nucleus formed at $t = 12000\delta t$; (b) the growth of the nucleus at $t = 25000\delta t$; (c) the growth of the nucleus at $t = 35000\delta t$; and (d) the growth of the nucleus at $t = 10^5\delta t$.

after the system's equilibrium. There are a lot of peaks, the positions of which fit fcc crystal structure (dashed line in Figure 1). Therefore, we can say that the final crystal structure formed in the system is mostly fcc, consistent with the observation of the middle panel. Seen from the middle panel of Fig. 1, the number of hcp and bcc particles first reach maximum and then decrease with the time steps. This means that some of hcp and bcc particles have been probably transformed into fcc particles in the late stage of crystallization. For a direct and clearer investigation of the dynamic process of fcc crystallization, Fig. 2 shows some snapshots of the system's nucleation during DPD simulation. Notice that only the largest cluster of solid-like particles is plotted, and that the red (blue, green) spheres represent fcc (bcc, hcp) particles. Fig. 2(a) gives the picture of the typical nucleus which has grown up into crystallite. Apparently fcc particles occupy the core of the nucleus, and there are very few hcp and bcc particles attached to this core. During the whole crystallization process, fcc particles are always dominant in the growing nucleus.

Upon increasing the density, the system goes through a fcc-bcc transition and it can be expected that bcc ordering will become dominant in the crystallites. In Fig. 3, the evolution of solid-like particles' number and RDF curve of the system at $T = 0.1$ and $\rho = 2.0$ are both shown. Obviously most of particles are in bcc ordering when the system has reached equilibrium, seen from the top panel of Fig. 3. The curve of averaged RDF also indicates this (see the bottom panel of Fig. 3), because the peaks of averaged RDF correspond to bcc structure. Some typical snapshots of a nucleation and its growth process are given in Fig. 4. In the earlier stage of the crystallization, the core of the nucleus is occupied by the mixture of fcc, hcp, and bcc particles, in which bcc particles are only slightly more than fcc and hcp particles (see Fig. 4(a)). Notice that the state point of $T = 0.1$ and $\rho = 2.0$ is near the boundary of fcc-bcc transition, so there are rather some fcc particles in the core of the nucleus. Nonetheless, the final configuration at equilibrium of the system is favorable for bcc phase. As the nucleus become bigger and bigger, the number of bcc particles is increased more rapidly than that of other types of solid-like particles. Finally bcc particles are dominant in the system when the crystallization is completed.

Such freezing behavior of soft particles is different from that of some colloidal systems, e.g., charged colloidal

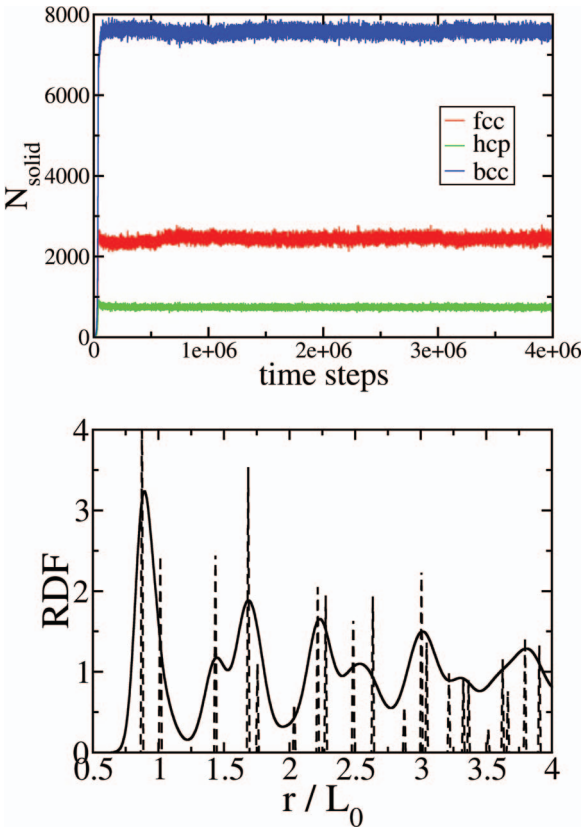

FIG. 3. Crystallization of bcc structure at $T = 0.1$ and $\rho = 2.0$. Top: the number of different types of solid-like (fcc, hcp, bcc) particles versus time step. Bottom: the curve of averaged RDF after equilibrium. The dashed lines in RDF curve indicate the peaks of perfect bcc crystal structure.

suspensions, where the bcc crystallization often appears before fcc crystallization when increasing the density.[31–33] The crystallization in colloids is usually attributed to excluded-volume effects because of hard interactions between particles. But the crystallization mechanism of harmonic spherical particles is different, because they have soft-repulsive, short-ranged, and bounded interactions. Another interesting feature of the system is that it exhibits reentrant melting upon being compressed to high density sufficiently. Actually the reentrant melting has also arisen in some other systems with bounded repulsive interaction, e.g., Gaussian core model and Hertzian spheres.[4,5,8] Fig. 5 shows the curve of averaged fraction of crystallization varying with the density at $T = 0.1$. Obviously, the system has a liquid state for $f_{crystal} \approx 0$ at both very low and high density, suggesting a reentrant melting transition. We notice that the effect of hysteresis (the choice of initial configurations) is not significant and it may only shift the boundary of phase transition slightly. Here we have compared our results with the phase diagram constructed via thermodynamic integration[10] (the phase regions are separated by dashed lines in Fig. 5). Seen from Fig. 5, our results of simulation are in agreement with observations by Zhu and Lu, i.e., the system undergoes liquid state, fcc crystallization, bcc crystallization, and reentrant melting phase transition as increasing the density. However, the reentrant melting density ($\rho \approx 2.3$) obtained by our DPD simulations is lower than the results by Zhu and Lu ($\rho \approx 2.65$), which means that our results show a smaller region of bcc phase.

When we continue to decrease the temperature, the phase behavior of the system becomes more complex. We find that the system tends to be trapped into glass phase when $T \leq 0.05$. Seen from Fig. 6, the system is arrested into an amorphous and disordered phase between $\rho = 2.0$ and $\rho = 2.2$ at $T = 0.05$, where the system should exhibit structural ordering according to the phase diagram constructed via thermodynamic integration.[10] In Fig. 7, the curve of the averaged RDF is given to show a typical amorphous structure at $T = 0.05$ and $\rho = 2.1$. We also calculate the MSD curve of the system where the amorphous phase appears to find that MSD almost reaches to a plateau indicating that the system jams and has shown a glass phase.

For some colloidal systems with short-range attractions, glass forming can happen when the particles are monodisperse because the attractions may drive the glass phase transition.[34–36] However, glass forming for most of the systems with soft particles often needs the particles to be bidisperse or polydisperse in order to avert the nucleation to the crystalline phase.[11,20,37–39] To our knowledge, there are few clean system with monodisperse soft particles which have glass forming. For instance, Ikeda and Miyazaki have recently investigated that the one-component GCM system vitrifies at very high densities, without polydispersity or bidispersity.[40,41] The glass forming in our system exists in the region of intermediate densities at low enough temperature. As the temperature is very low, $k_BT/\epsilon \ll 1$. The particles can only overlap at a significant energetic cost so as to make the soft particles to act similar to hard ones. Actually our glass forming may be comparable to the founding of Yukawa fluid by Robbins *et al.*, where the crystal nucleation is suppressed and Yukawa system tended to evolve into an amorphous phase when the repulsive interaction range decreased. Moreover, they observed that a frustrated glass state also happened near the bcc-fcc boundary where neither bcc nor fcc crystal structure was favored sufficiently for crystallization.[31]

In the context of classical nucleation theory (CNT), the rate I at which nuclei are formed is given by

$$I = \kappa \exp\left(-\Delta G^*/k_BT\right), \tag{11}$$

where ΔG^* is the maximum value of Gibbs free energy required to form a nucleus, and κ is a kinetic prefactor that is proportional to the self-diffusion coefficient D_f of the fluid. We have calculated the self-diffusion coefficient D_f at the temperature above the melting point where the system always exhibits a fluid state. Different from some simple liquids where D_f usually decreases monotonically with increasing number density, the harmonic spheres fluid exhibits a clear non-monotonic behavior. Such dynamical anomalies have been seen before in some other bounded potentials.[8,42,43] Interestingly, the minimum in D_f coincides with the starting point of the glass-like phase at $\rho = 2.0$ (see Fig. 8). So the jammed phase or glass formation appearing in the system seems to be attributed to the small value of the kinetic prefactor κ in the intermediate densities when decreasing the temperature low enough: it results in an extremely small nucleation rate to make a formation of the frustrated amorphous phase.

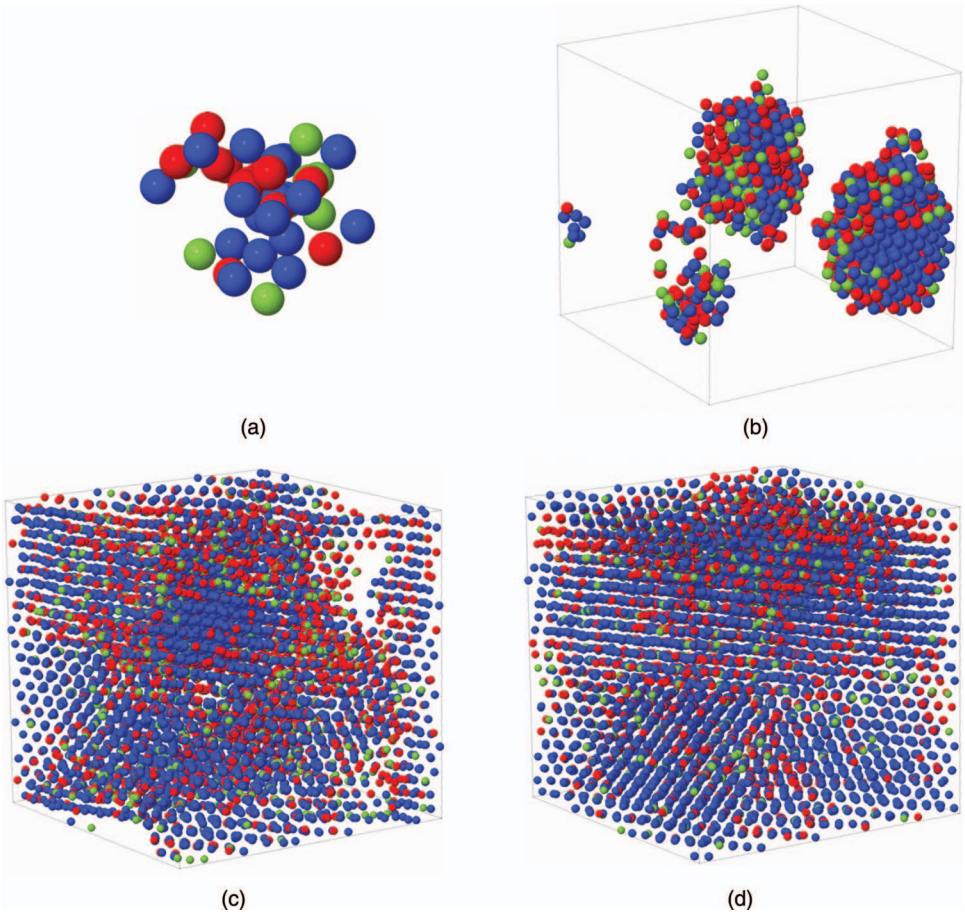

FIG. 4. Snapshots of bcc crystallization at $T = 0.1$ and $\rho = 2.0$. The symbol style is the same as Fig. 2. (a) The largest nucleus at $t = 15000\delta t$; (b) the growth of the nucleus at $t = 3 \times 10^4 \delta t$; (c) the growth of the nucleus at $t = 4 \times 10^4 \delta t$; and (d) the growth of the nucleus at $t = 10^5 \delta t$.

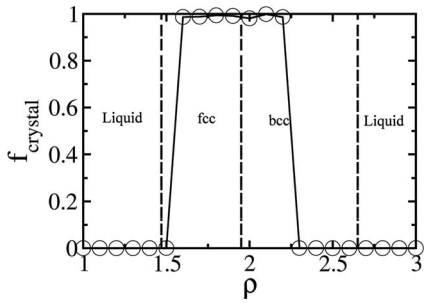

FIG. 5. Phase behaviors in different number density when $T = 0.1$. The circles and solid line represent the averaged fraction of crystallization after equilibrium. The dashed lines represent the boundary of liquid-fcc-bcc-liquid phase transition taken from Ref. 10.

Actually, D_f does not change that much over the range of the densities studied (especially the glass phase region $\rho = 2.0$–2.2 when $T = 0.05$), suggesting that the kinetic prefactors vary little correspondingly. Therefore, the influence of D_f on the glass forming is not significant at all. We notice that the glass phase transition happens near the fcc-bcc boundary. It is rather believed that glassiness is mainly due to the competition between two different crystalline phases which are roughly degenerate in chemical potential, actually making $\Delta G^*/k_B T$ increase drastically. In Fig. 4, we have already seen that the crystallization is started from a nucleus which is a mixture of fcc, hcp, and bcc particles near the fcc-bcc boundary at $T = 0.1$. Indeed the

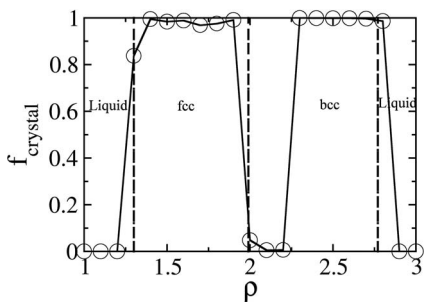

FIG. 6. Phase behaviors in different number density when $T = 0.05$. The symbol style is the same as Fig. 5.

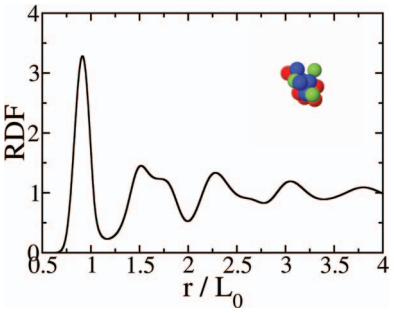

FIG. 7. RDF curve at $T = 0.05$ and $\rho = 2.1$. In inner panel, it shows the largest nucleus in the system at $t = 10^7 \delta t$.

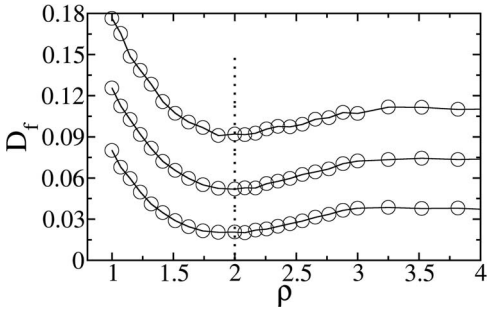

FIG. 8. Dependence of the diffusion coefficient D_f on the number density ρ at the temperatures slightly above the melting temperature. From bottom to top: $T = 0.2$, 0.3, 0.4. The dotted line shows the position $\rho = 2.0$ at which the jam starts when $T = 0.05$.

number of bcc particles is almost the same as that of fcc particles in the core of nucleus when the density approaches to the fcc-bcc boundary. The competition between fcc and bcc crystallization makes the nucleation rate rather small in this case. As the temperature is lower and lower, the nucleation rate will be even decreased and eventually it causes the system to vitrify. We have investigated the dynamics behavior of the system at $T = 0.05$ and $\rho = 2.1$, not finding any signs of crystallization. A few small nucleus may form and dissolve in the course of simulation, but none of them can grow up to crystallite. In the inner panel of Fig. 7, a largest nucleus at $t = 10^7 \delta t$ which consists of solid-like particles is shown, suggesting that the system does not crystallize even after very long time of simulation. For a further study, we have also tried to increase the temperature to $T > 0.05$ starting from the configuration of the glass forming. After some times steps, the small nucleus will become larger and larger to make the system crystallize finally, indicating that the nucleation rate is increased with the increasing of the temperature.

IV. CONCLUSION

DPD simulations are performed to investigate the dynamic process of crystallization or structural ordering in the system of soft particles interacting with harmonic repulsions. At the temperature just below the melting point, the system shows liquid state, fcc crystal structure, bcc crystal structure, and reentrant melting transition as increasing the density, which is in good agreement with the phase diagram constructed previously using thermodynamic integration. However, as the temperature is decreased sufficiently, the system is arrested in an amorphous state and exhibits a glass forming in the intermediate densities, where the phase diagram constructed via thermodynamic integration suggests a structural ordering.

ACKNOWLEDGMENTS

This work is supported by Grant Nos. 11172302, 20903112, 10972217, and 11032011 from the National Natural Science Foundation of China.

[1]C. N. Likos, Soft Matter **2**, 478 (2006).
[2]M. van Hecke, J. Phys.: Condens. Matter **22**, 033101 (2010).
[3]C. N. Likos, M. Watzlawek, and H. Lowen, Phys. Rev. E **58**, 3135 (1998).
[4]A. Lang, C. N. Likos, M. Watzlawek, and H. Lowen, J. Phys.: Condens. Matter **12**, 5087 (2000).
[5]S. Prestipino, F. Saija, and P. V. Giaquinta, Phys. Rev. E **71**, 050102(R) (2005).
[6]B. M. Mladek, D. Gottwald, G. Kahl, M. Neumann, and C. N. Likos, Phys. Rev. Lett. **96**, 045701 (2006).
[7]F. Saija, S. Prestipino, and G. Malescio, Phys. Rev. E **80**, 031502 (2009).
[8]J. C. Pamies, A. Cacciuto, and D. Frenkel, J. Chem. Phys. **131**, 044514 (2009).
[9]E. Lascaris, G. Malescio, S. V. Buldyrev, and H. E. Stanley, Phys. Rev. E **81**, 031201 (2010).
[10]Y. L. Zhu and Z. Y. Lu, J. Chem. Phys. **134**, 044903 (2011).
[11]N. Xu, T. K. Haxton, A. J. Liu, and S. R. Nagel, Phys. Rev. Lett. **103**, 245701 (2009).
[12]Z. X. Zhang, N. Xu, D. T. N. Chen, P. Yunker, A. M. Alsayed, K. B. Aptowicz, P. Habdas, A. J. Liu, S. R. Nagel, and A. G. Yodh, Nature (London) **459**, 230 (2009).
[13]G. Malescio, F. Saija, and S. Prestipino, J. Chem. Phys. **129**, 241101 (2008).
[14]G. Malescio, J. Phys.: Condens. Matter **19**, 073101 (2007).
[15]C. N. Likos, Phys. Rep. **348**, 267 (2001).
[16]F. H. Stillinger, J. Chem. Phys. **65**, 3968 (1976).
[17]C. N. Likos, A. Lang, M. Watzlawek, and H. Lowen, Phys. Rev. E **63**, 031206 (2001).
[18]D. J. Durian, Phys. Rev. Lett. **75**, 4780 (1995).
[19]C. S. O'Hern, S. A. Langer, A. J. Liu, and S. R. Nagel, Phys. Rev. Lett. **88**, 075507 (2002).
[20]L. Berthier, H. Jacquin, and F. Zamponi, Phys. Rev. E **84**, 051103 (2011).
[21]N. B. Wilding, Mol. Phys. **107**, 295 (2009).
[22]H. Jacquin and L. Berthier, Soft Matter **6**, 2970 (2010).
[23]J. Mattsson, H. M. Wyss, A. Fernandez-Nieves, K. Miyazaki, Z. B. Hu, D. R. Reichman, and D. A. Weitz, Nature (London) **462**, 83 (2009).
[24]R. D. Groot and P. B. Warren, J. Chem. Phys. **107**, 4423 (1997).
[25]G. A. Mcconnell, A. P. Gast, J. S. Huang, and S. D. Smith, Phys. Rev. Lett. **71**, 2102 (1993).
[26]I. W. Hamley, C. Daniel, W. Mingvanish, S. M. Mai, C. Booth, L. Messe, and A. J. Ryan, Langmuir **16**, 2508 (2000).
[27]J. Russo and H. Tanaka, Soft Matter **8**, 4206 (2012).
[28]P. J. Hoogerbrugge and J. M. V. A. Koelman, Europhys. Lett. **19**, 155 (1992).
[29]P. Español and P. Warren, Europhys. Lett. **30**, 191 (1995).
[30]P. R. ten Wolde, M. J. RuizMontero, and D. Frenkel, J. Chem. Phys. **104**, 9932 (1996).
[31]M. O. Robbins, K. Kremer, and G. S. Grest, J. Chem. Phys. **88**, 3286 (1988).
[32]L. Gu, S. Xu, Z. Sun, and J. T. Wang, J. Colloid Interface Sci. **350**, 409 (2010).
[33]S. H. Xu, H. W. Zhou, Z. W. Sun, and J. C. Xie, Phys. Rev. E **82**, 010401 (2010).
[34]E. Zaccarelli, G. Foffi, F. Sciortino, P. Tartaglia, and K. A. Dawson, Europhys. Lett. **55**, 157 (2001).
[35]K. A. Dawson, G. Foffi, F. Sciortino, P. Tartaglia, and E. Zaccarelli, J. Phys.: Condens. Matter **13**, 9113 (2001).
[36]K. A. Dawson, Curr. Opin. Colloid Interface Sci. **7**, 218 (2002).
[37]L. Berthier and T. A. Witten, Europhys. Lett. **86**, 10001 (2009).
[38]H. Jacquin, L. Berthier, and F. Zamponi, Phys. Rev. Lett. **106**, 135702 (2011).
[39]M. Schmiedeberg, Phys. Rev. E **87**, 052310 (2013).
[40]A. Ikeda and K. Miyazaki, Phys. Rev. Lett. **106**, 015701 (2011).
[41]A. Ikeda and K. Miyazaki, J. Chem. Phys. **135**, 054901 (2011).
[42]G. Foffi, F. Sciortino, P. Tartaglia, E. Zaccarelli, F. Lo Verso, L. Reatto, K. A. Dawson, and C. N. Likos, Phys. Rev. Lett. **90**, 238301 (2003).
[43]W. P. Krekelberg, T. Kumar, J. Mittal, J. R. Errington, and T. M. Truskett, Phys. Rev. E **79**, 031203 (2009).